Journal of
Nanoscience and Nanotechnology
Vol. 8, 1–6, 2008

Magnetic Properties of Barium Ferrite Dispersed Within Polystyrene-Butadiene-Styrene Block Copolymers

M. Chipara[1,*], R. Skomsky[2], N. Ali[3], D. Hui[4], and D. J. Sellmyer[2]

[1] *Department of Physics and Geology, University of Texas—Pan American, Edinburg, TX 78541, USA*
[2] *Department of Physics, University of Nebraska, Lincoln, NE-68588, USA*
[3] *Department of Mechanical Engineering, University of Aveiro, Portugal*
[4] *Department of Mechanical Engineering, University of New Orleans, New Orleans, LA, USA*

Magnetic properties of nanocomposite materials obtained by dispersing barium ferrite nanoparticles within polystyrene-butadiene-styrene block copolymer, in the temperature range, 300 to 500 K are reported. The temperature dependence of the magnetization at saturation, averaged uniaxial magnetocrystalline anisotropy, and coercive field of thick films are analyzed. A "matrix effect" was noticed within the glass transition range of the hard component (polystyrene) of the polymeric matrix. The reported modifications of the magnetic properties were assigned to the competition between the magnetic and mechanical reorientation of nanoparticles within the polymeric matrix. Such modifications were not observed in barium ferrite dispersed in cement.

Keywords: Magnetic Nanoparticles, Block Copolymer, Magnetocrystalline Anisotropy, Coercive Field, Matrix Effect.

RESEARCH ARTICLE

1. INTRODUCTION

Nanomagnetism attracted much interest derived from the novel magnetic behavior resulting from the nanometer scale confinement of magnetic moments[1,2] and by the wide variety of applications ranging from ultra high density magnetic media[3] to biology and medicine.[4,5]

As in macroscopic magnetic samples, the magnetization's orientation of magnetic nanoparticles is controlled by the free energy minim. Accordingly, most magnetic nanoparticles are either single domain or exhibit superparamagnetic features.[1,2,6,7] The dispersion, trapping, and orientation of magnetic nanoparticles in polymeric matrices have potential applications in future ultra high density storage devices,[3] nanocompasses,[2,7] and controlled drug release.[4,5] The dynamics of magnetic nanoparticles within polymers reflects the competition between the reorientation of magnetic moments in external magnetic fields[8] and the mechanical reorientation of the whole particle.

The reorientation of magnetization in magnetic nanoparticles. The Hamiltonian H[9] describes reorientation magnetic nanoparticles placed in an external magnetic field H:

$$\mathcal{H} = -\sum_{m=n} J_{mn} S_m S_n - \mu_0 \sum_m H S_m - \mu_0 \sum_{m=n} \frac{3(S_m e_{mn})(S_n e_{mn}) - (S_m S_n)}{r_{mn}^2} - K \sum_n V_n \frac{(S_n k_n)^2}{|S_n|^2} \quad (1)$$

Where S is the electronic spin of isolated nanoparticle, J the exchange integral between two electronic spins S_n and S_m, V_n the volume of the nth particle, K the anisotropy constant, k_n the unit vector along the easy axis of magnetization for the ferromagnetic nanoparticle, r_{nm} is distance between the two spins (or between the two magnetic particles), and e_{nm} the unit vector pointing along r_{nm}. The second term describes the reorientation of the direction of the magnetization of a magnetic particle in external magnetic field. Only the last term couples the orientation of the electronic spins with the lattice of the particle, through the magnetocrystalline anisotropy. In conclusion, for magnetic particles with negligible magnetocrystalline anisotropy or

*Author to whom correspondence should be addressed.

shape anisotropy (such as spherical nanoparticles[10, 11]), there is no connection between the magnetic reorientation of electronic spins and mechanical reorientation of the particle.

Gilbert equation[12] describes the reorientation of magnetization M in external magnetic fields:

$$\frac{dM}{dt} = \gamma(M \times H_{\text{eff}}) - \frac{\alpha}{M_S}\left(M \times \frac{dM}{dt}\right) \quad (2)$$

Where γ is the gyromagnetic ratio, α describes the magnetic viscous damping of the magnetization evolution, and H_{eff} is the effective local magnetic field. The average magnetization at saturation $\langle M_S \rangle$ of a randomly oriented ensemble of magnetic particles in an external magnetic field of intensity H is.[12]

$$\langle M_S \rangle = \frac{2p}{3}\frac{M_S(T)}{H_a(T)}H \quad (3)$$

Where p is the packing fraction of the powder, and H_a is the anisotropy field of nanoparticles.

The mechanical reorientation of the whole magnetic nanoparticle. The relaxation time, τ, characteristics to the mechanical reorientation of nanoparticles depends on their volume (V), on the viscosity (η) of the medium in which they are embedded, and on temperature (T):

$$\tau = \frac{6V\eta}{K_B T} \quad (4)$$

Particles and molecules with volumes ranging between 10^{-3} nm^3 and 10^3 nm^3 can move freely within polymeric matrices. Spin probe investigations revealed that these motions can be deconvoluted into random jumps and particle rotations.[13] For polymeric matrices within the glass transition temperature (T_G), the temperature dependence of viscosity shows a deviation from the usual Arrhenius like dependence, defined by the WLF equation:[13, 14]

$$\ln\frac{\eta}{\eta(T_G)} = -\frac{C_{1g}(T - T_G)}{C_{2g} + T - T_G} \quad (5)$$

Where C_{1g} and C_{2g} are constants. Equation (5) is valid in the temperature range T_G, $T_G + 120$ K. A size dependent shift of T_G for small molecules dispersed within polymeric matrices has been suggested[14] and an apparent glass transition temperature (T_{GA}) that scales the dynamical characteristics of nanoparticles to the glass transition temperature (T_G) of the polymer has been introduced. Below T_{GA} the thermal motions of nanoparticles are frozen. As the temperature is raised above T_{GA} thermal motions of nanoparticles are excited.

For magnetic nanoparticles characterized by strong electron spin–lattice coupling (with large magnetocrystalline or shape anisotropy) a coupling between the magnetic and mechanical reorientations is expected.

The free magnetic rotator behavior, reported[2, 7] for magnetic nanoparticles dispersed in various fluids (including polymers) at temperature lower (or equal) to the room temperature will allow also the orientation of magnetic nanoparticles within polymeric matrices. Such nanoparticles rotate freely within nanometer sized cages in low viscosity fluids (or polymers). The rotation occurs along the equilibrium direction, which is the direction of the external applied magnetic field. While the role of dipolar interactions[1, 9] on the evolution of magnetic nanoparticles dispersed in fluids is generally accepted, recent studies[1] suggest that Van der Waals interactions may also contribute to the reorientation of magnetic nanoparticles through the formation of the chain-like magnetic structures. Recent phenomena such as the surface mediated magnetic anisotropy[12, 15] complicates the analysis of the evolution of magnetic nanoparticles dispersed within polymeric matrices.

The goal of the present study is to investigate the coupling between magnetic (spin) reorientation and mechanical reorientation for nanoparticles with high magnetocrystalline anisotropy dispersed within polymeric matrices.

2. EXPERIMENTAL DETAILS

Barium ferrite, BaFe ($BaFe_{12}O_{19}$) is a ferrimagnetic material characterized by high Curie temperature ($T_C = 723$ K), large magnetic moment ($\mu_0 M_S = 0.48$ T), high coercivity at room temperature (140 to 165 kA/m), high energy product (about 25 kJm^{-3}), large first order magnetocrystalline uniaxial anisotropy (of about 250 kJm^{-3}), and good thermal stability.[16, 17] The crystalline structure of barium ferrite is hexagonal.[18] BaFe has been already used in magnetic data storage.[16–22] BaFe nanoparticles are among the potential materials for future ultra high-density data storage.[16, 17, 20–22] Due to the large magnetocrystalline and shape anisotropy and to the high Curie temperature, such particles should be magnetic at nanometer scale and room temperature, providing an excellent magnetic system for the investigation of the coupling between magnetic and mechanical reorientation. In order to obtain magnetic nanoparticles, barium dodecairon nanodecaoxide powder ($BaFe_{12}O_{19}$ or barium ferrite), from Aesar has been subjected to energetic mechanical milling. The particle size has been estimated by Wide Angle X-Ray Scattering (WAXS) using a Rigaku X-Ray Diffractometer.

Nanoparticles of BaFe were dispersed into a block copolymer based on polystyrene and polybutadiene, which presents two glass transition temperatures,[13] one at about 213 K and the other at about 373 K assigned to the onset of molecular motions in the soft (polybutadiene) and hard (polystyrene) phases, respectively. Ba-Fe nanoparticles have been mixed with dilute solutions of polystyrene-butadiene-styrene block copolymer (SBS) in toluene and

sonicated at room temperature for about 30 hours. The research grade polymer and solvent have been purchased from Aldrich. Films of BaFe-SBS have been obtained by dripping the sonicated mixture of BaFe and SBS in toluene onto microscope slides, followed by solvent evaporation. Solvent's traces have been removed by heating the samples in vacuum at 325 K for 24 hours. BaFe nanoparticles have been also dispersed within Thermeez Ceramic Putty, provided by Cotronics Corp (cement-BaFe). This putty presents no phase transitions up to about 600 K.

The temperature dependence of the magnetization has been measured by using a vibrational sample magnetometer (VSM) manufactured by Lake Shore. VSM measurements on the same BaFe nanoparticles (average diameter of about 17 nm) dispersed within cement (BaFe-cement) have been performed to accurately assess matrix effects. In order to prevent the melting of the sample, the highest temperature of BaFe-SBS was limited to 500 K.

3. RESULTS AND DISCUSSION

WAXS spectra of milled BaFe particles (for various milling times) are shown in Figure 1(A). The size of BaFe nanoparticles was calculated from the width of WAXS spectra, assuming Lorentzian like diffraction lines. The particle size along a direction normal to the hkl plane (d_{hkl}) has been determined from the width at half intensity of the corresponding (hkl) diffraction line W_{hkl}, by using the expression:[18]

$$d_{hkl} = \frac{0.91\lambda}{W_{hkl}\cos\theta_{hkl}} \quad (6)$$

Where λ is the wave length of the incoming X-ray radiation and θ_{hkl} is the diffraction angle for the hkl plane. The line width has been corrected for instrumental broadening. The particle size has been estimated from the width of the most intense line, corresponding to (114) planes.[18]

Figure 1(B) depicts the dependence of particle size on the milling time. It is noticed that the size of magnetic nanoparticles decreases as the milling time is increased reaching an asymptotic value of about 13 nm, after milling times longer or equal to 30 minutes.

For a better understanding of the coupling between magnetic and mechanical reorientation processes, a thorough investigation of the temperature behavior of the hysteresis loops of BaFe-SBS and BaFe-cement nanocomposites has been performed. VSM measurements were conducted on thick samples (thickness of about 1 mm), containing the same weight concentration of BaFe (5% wt in SBS and cement, respectively). No differences between the WAXS patterns (peaks position, amplitude, and width) of BaFe embedded within SBS and cement were noticed (within experimental errors).

The hysteresis loops of SBS-BaFe and SBS-cement after the subtraction of the paramagnetic contributions are shown in Figure 2. Small changes in the hysteresis loops of BaFe-SBS composites around $H = 0$ are noticed in Figures 2 and 3. The differences are more obvious in the plot of the first derivative of sample magnetization (with respect to the intensity of the magnetic field; dM/dH) versus the magnetic field intensity. The presence of a peak in these plots indicates an inflection point on the hysteresis loop. It is observed that BaFe-SBS composites present

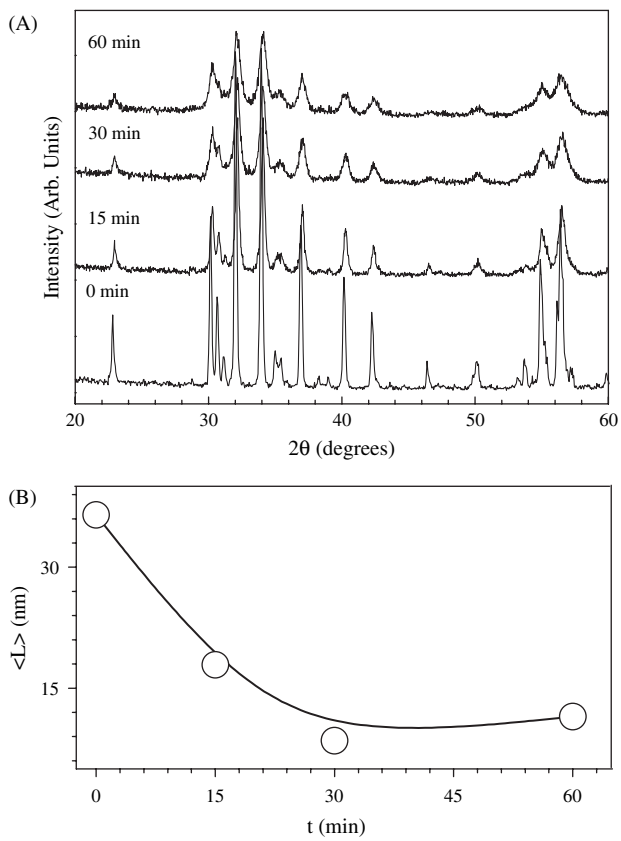

Fig. 1. (A) X-ray diffractograms of BaFe-SBS nanoparticles after different milling times. (B) The dependence of particle size on milling time, as estimated from the width of X-ray diffraction spectra (see Eq. (6)).

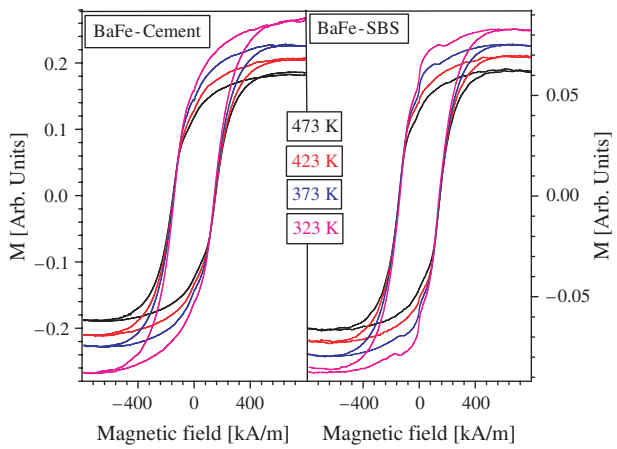

Fig. 2. The hysteresis loops of BaFe-SBS nanocomposites and BaFe-cement at various temperatures.

RESEARCH ARTICLE

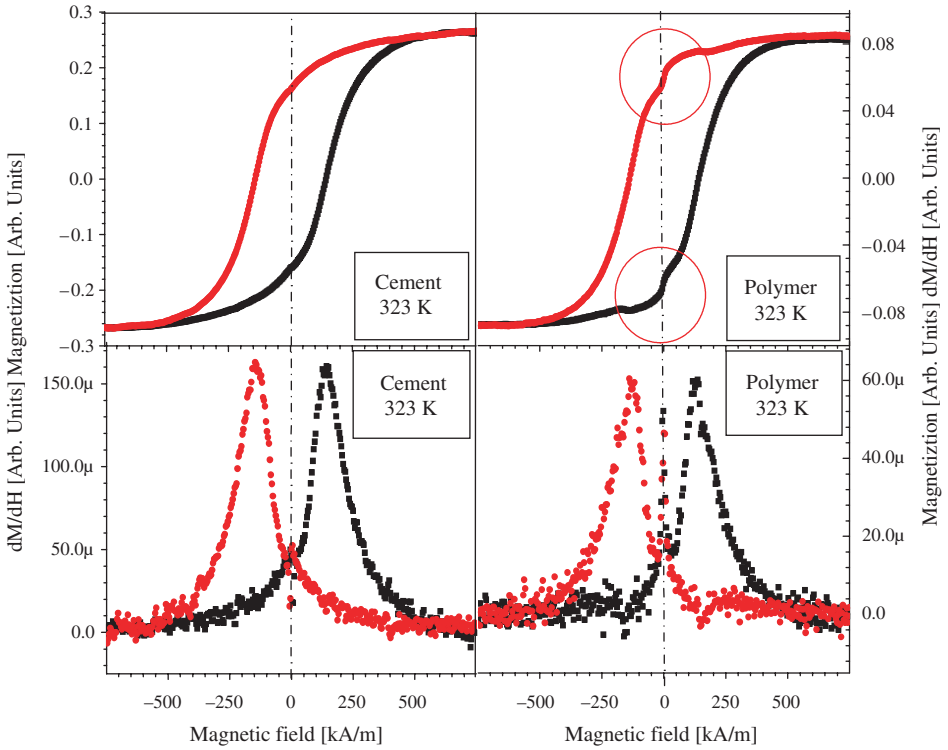

Fig. 3. The hysteresis loop of Ba-Fe cement (left panel) and BaFe-SBS at 50 °C. The upper panels show the hysteresis loops while the bottom panel shows the first derivative of the hysteresis loops relative to the magnetic field strength's.

two peaks (in the dM/dH plot vs. H) one located at values closed to the coercive field, named peak field (H_P), and the other located near zero applied magnetic field. H_P may be defined also as half of the projection of the distance between the extreme inflection points of the hysteresis loop onto the external (applied) magnetic field axis. The second peak is almost absent in BaFe-cement composites. This behavior resembles the reported hysteresis loops of free magnetic nanoparticles in polymers.[7,10] However, there is a noticeable difference; the results reported here were obtained at high temperatures and without a prior magnetic treatment of the sample. As the size, concentration, and distribution of magnetic nanoparticles is identical in both BaFe-SBS and BaFe-cement samples, the observed difference noticed near $H = 0$ (which are consistent with a larger contribution of superparamagnetic particles or free nanomagnetic rotors in the BaFe-SBS composite) were assigned to the coupling between mechanical reorientation (sensitive to segmental motions) and magnetic reorientation of nanoparticles. While the magnetic nanoparticles are almost frozen within the BaFe-cement sample, the barium ferrite nanoparticles located in the polybutadiene phase (which is in the high elastic state at room temperature[13]) are subjected to thermal activated jumps which average their intrinsic magnetic properties enhancing the weight of the superparamagnetic phase. However, the nanoparticles trapped in the polystyrene domains are pinned at nanometer scale (as the segmental motions in this phase are frozen). The segmental motions of the polystyrene phase are activated around 380 K.[13]

The temperature dependence of the coercive field (H_C) and peak field (H_P) for both samples is shown in Figure 4. In pristine and doped BaFes, the temperature dependence of the coercive field may be complex (not monotonous).[22,23] This derives from the interactions between the magnetic moments located on the two sublattices as well as from the fact that the coercive field in BaFes results from

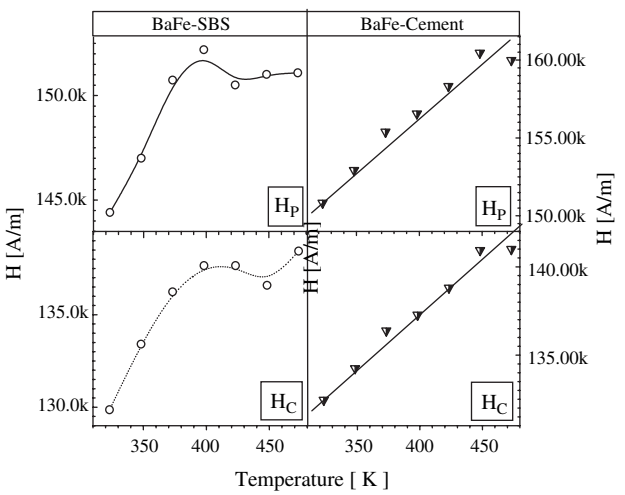

Fig. 4. The temperature dependence of the coercive field (H_C) and of the peak field (H_P).

the competition between the temperature dependence of the shape anisotropy (expressed by NM_S) and of magnetocrystalline anisotropy (defined by $2K_1/\mu_0 M_S$):[19, 21]

$$H_C = \alpha\left(\frac{2K_1}{\mu_0 M_S} - NM_S\right) \tag{7}$$

The differences between the SBS and cement matrices are clearly shown in Figure 4. It is observed that both H_C and H_P have analogous temperature dependencies and that there is a significant departure between these dependencies; in the case of the polymeric (SBS) matrix, a maximum is noticed at 400 K (within the glass transition range of the polystyrene phase). The small shift in the glass transition temperature from about 373 K to 400 indicates that the volume of nanoparticles is larger than the segmental volume.[14]

The dependence of the magnetization on the external magnetic field, at large magnetic fields (over 1 T) was fitted using (8), after extracting a linear contribution due to the diamagnetic and paramagnetic contributions:[21]

$$M(H) = M_S^0\left[1 - \frac{A}{H} - \left(\frac{B}{H}\right)^2\right] + \chi_P H \tag{8}$$

Where H represents the strength of the external magnetic field. The term A/H has been assigned to strain field around dislocations or to paramagnetic impurities. The term $(B/H)^2$ collects the overall anisotropy of the sample (shape, magnetocrystalline, and strain anisotropy). As noticed from Figure 5, the paramagnetic correction χ_P obeys a Curie like temperature dependence (see the left bottom panel Fig. 5). This self consistent analysis confirms the accuracy of the deconvolution of paramagnetic defects from ferromagnetic contributions. A detailed analysis of this dependence showed that the contribution of the A/H term is rather small in comparison with the $(B/H)^2$ term. It was reported that in bulk BaFe the term A/H is negligible in comparison with $(B/H)^2$. In Figure 5 it is shown, in arbitrary units, the temperature dependence of the A term (see the right top panel). The Curie-like behavior suggests that in this case paramagnetic or superparamagnetic contributions are dominant. The temperature dependence of B is shown in the right bottom panel of Figure 5.

For hexagonal ferrites, B is proportional to the anisotropy field H_a, which is dominated by the first order magnetocrystalline anisotropy, K_1.[16, 21]

$$B \approx \frac{H_a}{\sqrt{15}} = \frac{2K_1}{\sqrt{15}M_S} \tag{9}$$

From Figure 5 it is noticed that at high temperatures the value of B for BaFe-polymer are smaller than the corresponding values for BaFe-cement.

The fact that the magnetization at saturation of BaFe-SBS is larger at high temperatures than the magnetization at saturation of BaFe-cement may express a better

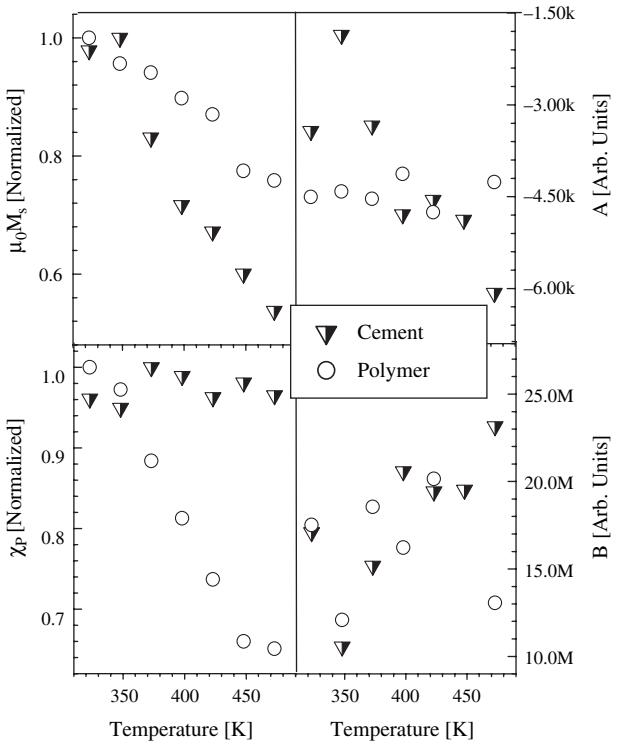

Fig. 5. Left upper panel: The dependence of the magnetization at saturation on temperature for both BaFe-SBS and BaFe-Cement. Right upper panel: The temperature dependence of A (as estimated from Eq. (8) for both BaFe-SBS and BaFe-cement). Left bottom panel: The temperature dependence of the paramagnetic susceptibility, as estimated from Eq. (8) for both BaFe-SBS and BaFe-cement). Right bottom panel: The temperature dependence of B (as estimated from Eq. (8) for both BaFe-SBS and BaFe-cement).

averaging of the magnetocrystalline anisotropy due to the contributions of the segmental motions, as long as according to Eq. (3) p is the same for BaFe-SBS and BaFe-cement. According to Eq. (3) proposed for the average magnetization of magnetic nanocomposites, the decrease of the intensity of the anisotropy field H_a though particle reorientation processes leads to an enhancement of the average magnetization at saturation. This conclusion is supported by the fact that at high temperature the term B (for BaFe-SBS) is smaller than the value of B for BaFe-cement.

This conclusion reveals again the impact on segmental motions on the magnetic properties of the nanocomposite. Equation (9) has been used to estimate the temperature dependence of the axial magnetocrystalline anisotropy, shown in the bottom panel of Figure 6. It is noticed that the shape anisotropy is decreased as the temperature is increased. This result from the competition of two processes, one intrinsic related to the temperature dependence of the magnetization at saturation within magnetic nanoparticles and the second associated to the increase of the molecular motions of the matrix, that may result in an improved averaging of the local field anisotropies. At room temperature the estimated value of K_1 is about 30% of

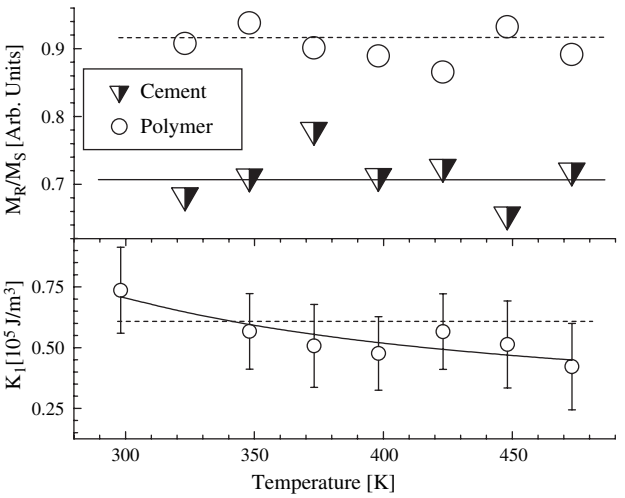

Fig. 6. Bottom panel: The temperature dependence of the magnetocrystalline anisotropy of BaFe in BaFe-SBS nanocomposites as estimated from Eq. (9). Upper panel: The temperature dependence of the squareness of hysteresis loops for BaFe-SBS and BaFe-cement.

the value reported in bulk barium ferrite,[19, 21] confirming the random distribution of particle directions in space. The temperature dependence of the average value of uniaxial magnetocrystalline anisotropy $\langle K_1 \rangle$ obeys an Arrhenius like dependence on temperature,[21, 22] as shown by the bold line in Figure 6.

$$\langle K_1 \rangle = \langle K_1^0 \rangle \exp -\frac{E_A}{K_B T} \tag{10}$$

The estimated activation energy E_A, corresponding to the best fit is about $3.0 \times 10^{12} \pm 0.2 \times 10^{12}$ J/kMole (or about 5×10^{-8} ergs). The average extrapolated value of uniaxial anisotropy was $\langle K_1^0 \rangle = 0.21 \times 10^5$ J/m^3.

The temperature dependence of the hysteresis loop squareness is shown in the top panel of Figure 6. While it is possible to accept that the squareness of the hysteresis loop is almost temperature independent (within experimental errors), it is noticed that the squareness of BaFe-SBS is larger than the squareness of BaFe-cement, reflecting a better averaging of M_S and accordingly a smaller magnetization at saturation in the BaFe-SBS composite.

4. CONCLUSIONS

The coupling between magnetic and mechanical reorientation process for magnetic nanoparticles of BaFe dispersed within a blockcopolymer has been reported. Experimental data showed an anomaly in the temperature dependence of the coercive field of BaFe-SBS composite near the glass transition temperature of the hard phase (polystyrene), which was assigned to the coupling between mechanical and magnetic reorientation process. The conclusion is supported by the absence of this anomaly for the BaFe-cement system.

Acknowledgments: This research has been supported by NSF and by Nebraska Center for Materials and Nanoscience.

References and Notes

1. Y. Lalatonne, J. Richardi, and M. P. Pileni, *Nat. Mater.* 3, 121 **(2004)**.
2. A. M. Testa, S. Foglia, L. Suber, D. Fiorani, L. I. Casas, A. Roig, E. Molins, and J. M. Greneche, *J. Appl. Phys.* 90, 1534 **(2001)**.
3. D. Goll, A. E. Berkowitz, and H. N. Bertram, *Phys. Rev. B* 70, 184432 **(2004)**.
4. P. Gold, *Mater. Today* 2, 36 **(2004)**.
5. R. E. Edelman and R. Langer, *Biomaterials* 14, 621 **(1993)**
6. R. H. Kodama, *J. Magn. Magn. Mat.* 200, 359 **(1999)**.
7. R. D. Zysler, J. Tejada, and E. Molins, *J. Magn. Magn. Mat.* 272–276, 1191 **(2004)**.
8. D. Braun, *J. Magn. Magn. Mat.* 283, 1 **(2004)**.
9. L. Subhalakshmi, *Phys. Stat. Sol. (b)* 241, 3022 **(2004)**.
10. T. Leineweber and H. Kronmuller, *Physica B* 275, 5 **(2000)**.
11. M. Chipara, R. Skomski, and D. J. Sellmyer, *J. Magn. Magn. Mat.* 249, 246 **(2002)**.
12. P. C. Fannin, B. K. P. Scaife, A. T. Giannitsis, and S. W. Charles, *J. Phys. D: Appl. Phys.* 35, 1305 **(2002)**.
13. M. Chipara, C. C. Rowlands, and A. N. Galatanu, *J. Polym. Sci.: Part B: Polym. Phys.* 42, 1960 **(2004)**.
14. M. Chipara, *Physica B* 234–236, 263 **(1997)**.
15. A. Snezhko, I. S. Aranson, and W. K. Kwok, *Phys. Rev. E* 73, 041306 **(2006)**.
16. G. Mendoza-Suárez, J. A. Matutes-Aquino, J. I. Escalante-García, H. Mancha-Molinar, D. Ríos-Jará, and K. K. Johal, *J. Magn. Magn. Mat.* 223, 55 **(2001)**.
17. M. Pal, S. Bid, S. K. Pradhan, B. K. Nath, D. Das, and D. Chakravorty, *J. Magn. Magn. Mat.* 269, 42 **(2004)**.
18. W. D. Townes, J. H. Fang, and A. J. Perrotta, *Z. Krystallogr., Krstallgeom., Krystallphys, and KristallChem.* 11, 125 **(1967)**.
19. F. L. Wei, M. Lu, and Z. Yang, *Phy. Stat. Sol. (a)* 169, 303 **(1998)**.
20. H. C. Fang, Z. Yang, C. K. Ong, and C. S. Wang, *J. Magn. Magn. Mat.* 187, 129 **(1998)**.
21. M. Chipara, D. Hui, J. Sankar, D. Leslie-Pelecky, A. Bender, L. Yue, R. Skomski, and D. J. Sellmyer, *Composites B* 35, 235 **(2004)**.
22. H. Pfeiffer and W. Schuppel, *J. Magn. Magn. Mat.* 130, 92 **(1994)**.
23. L. P. Ol'khovik, M. M. Khvorov, N. M. Borisova, Z. V. Golubenko, S. I. Sizova, and E. V. Shurinova, *Phys. Solid State* 45, 675 **(2003)**.

Received: 2 September 2007. Accepted: 22 November 2007.

RESEARCH ARTICLE